Direct Synthesis of Graphene Layers on a final use surface. A study of the Morphologies obtained on fiberglass using a non-thermal plasma system

Rafael Nogueira Bonifácio

rafaelnbonifacio@gmail.com

Instituto de Pesquisas Energéticas e Nucleares

Barbara Perez Gonçalves Silva

Instituto de Pesquisas Energéticas e Nucleares

Larissa Otubo

Instituto de Pesquisas Energéticas e Nucleares

Rodrigo Fernando Brambilla de Souza

Instituto de Pesquisas Energéticas e Nucleares

Almir Oliveira Neto

Instituto de Pesquisas Energéticas e Nucleares

Dolores Ribeiro Ricci Lazar

Instituto de Pesquisas Energéticas e Nucleares

Research Article

Keywords: graphene, instantaneous synthesis, direct application on surfaces, cyclohexane, button up approach

Posted Date: May 6th, 2025

DOI: https://doi.org/10.21203/rs.3.rs-6290494/v1

Additional Declarations: No competing interests reported.

Abstract

The simultaneous synthesis and application of graphene layers (graphenoid) materials directly onto a surface, or the direct construction of specific structures with this kind of material, could lead to significant developments in various scientific fields. In this study, graphene layers were synthesized directly applied to a target surface using an instantaneous reduction method based on the incidence of an electric arc that reduce cyclohexane vapor on the surface. The surface evaluated was fiberglass, a material with a curved shape and high contact angle, representing a challenging or even worst-case scenario for such depositions. As a result of process features, as well as its evaluation at different time intervals, graphene layered structures with varying shapes, thicknesses, roughness, porosities, and topographical profiles were obtained. Furthermore, the obtaining of compact and mechanically resistant structures was also observed. Throughout the study, the key attributes of this method were presented and discussed, demonstrating its potential to advance the field of direct graphene-based materials synthesis and application.

1. Introduction

Graphene remains being a material of great interest for various applications, due to its excellent properties such as mechanical strength (1,060 GPa), thermal conductivity (~5,000 W m^{-1} K^{-1}), electron mobility (2 10^5 cm^2 V^{-1} s^{-1}), Young's modulus (~1 TPa), surface area (2,630 m^2 g^{-1}) and electrical conductivity (~2,000 S m^{-1}) among others [1]. Thus the development of methods to produce graphene structures with high quality in a clean way remain been a technological demand for further developments.

Numerous studies have evaluated the production of graphene or few layers graphene (graphenoid) materials through discharge arc technologies [2–9]. In these works, different experimental setups and process approaches have been evaluated and resulted in materials with different characteristics. According to them, factors such as reaction chambers and electrodes (design and materials) [3–9], arc distance and gradient of temperature around it [5, 6], applied current [7], carbon source (C_3H_8 [3], CH_4 [4], graphite [5, 9]), presence of chemicals as buffer gases (Ar, He, N_2, H_2, NH_3, CO_2 and air in different concentrations our mixtures [2–9]), system pressure [3–5], and even the use of magnetic field [3], resulted in graphene-like materials with different characteristics in terms of composition, morphology, number of layers, and defects. According to some of these studies, these variables also influence the materials purity [9], crystallinity [5], specific surface area [3, 5] and oxidation resistance [9].

In a previous study [10], we demonstrated the production of graphene flakes in a single step using a “bottom-up” approach with cyclohexane as the carbon source in a non-thermal plasma system. The experiment was conducted in a two-neck volumetric flask, where a voltaic arc was generated between a 316L steel electrode and a mineral graphite electrode, both immersed in cyclohexane under an N_2 atmosphere [10]. Additionally, it was verified that graphene could be produced directly applied on a substrate’s surface, eliminating the need for steps such as inks preparation and application. Therefore,

this development may enable specific applications of graphene, particularly in scenarios where ink-based methods are not feasible. Furthermore, compared to chemical routes, this method is faster, generates no liquid waste and reduces costs in graphene production [10].

In this work, as a next step in our development, we modified the experimental setup and increased system dimensions. The reaction chamber was adjusted in both size and shape, and the electrodes were modified in terms of material, size and shape. The addition of the carbon source was changed from using a reaction chamber filled with liquid cyclohexane to a chamber containing cyclohexane vapor. Additionally, studies were conducted on graphene depositions using different process times in order to explore the new experimental setup for obtaining different types of deposits. These studies aimed to analyze the structures and morphologies produced by the technique and to gather more information about the process features.

The use of fiberglass as substrate for method evaluation is particularly interesting due to its properties, such as mechanical strength, lightness and durability [10–12], as well as its extensive application in sectors like construction, automotive, and aerospace industries [10, 13–15]. These applications could potentially be expanded to others sectors and technologies through the combination of fiberglass and graphene layers properties. Furthermore, fiberglass has a curvy shape and exhibits hydrophobic behavior [10], which tends to hinder the application of other materials on its surface. Thus, the method is being evaluated under a kind of worst-case scenario.

2. Experimental

2.1 – Direct graphene synthesis

In this study, the reaction chamber used was a cylindrical glass electrochemical cell with a diameter around 18 cm and a height of 12 cm. Its lid had openings with a diameter of ~ 1.0 cm, which allowed the passage of electrical wires and hoses for supplying reagents, and were closed with a polymeric film. In this chamber, two electrodes (graphite plates) with face dimensions of approximately 7.0 x 4.0 cm and thickness of 2.0 cm were parallelly positioned, with a distance of around 2.0 cm between their surfaces. The substrate to receive the direct synthesis of graphene layers (also referred to as “deposition” hereafter) was placed on a electrode surface and exposed to the inert atmosphere. The carbon source (cyclohexane vapor) was introduced by adding ~ 1.0 ml of liquid cyclohexane (analytical grade, from Aldrich) into the reaction chamber per minute of experiment, allowing it to evaporate. Nitrogen (N_2) was used as the inert gas. The *Fiberglass-E-glass* substrate (54% SiO_2, 14% Al_2O_3, 6% B_2O_3, 22% CaO, and traces of MgO, K_2O, Na_2O, Fe_2O_3 and F_2, each below 1%) [10] was purchased from *Casa da Resina* - Belo Horizonte, Brazil.

A 60 kW DC power generator [10] was connected to both electrodes, to establish a potential difference between them generating voltaic arcs, to reduce the reactant vapor forming solid materials. Such deposition procedure was performed at durations of 5, 10 and 30 minutes. These samples were

respectively designated as fiberglass with short time deposition (Fg-Short-dep), fiberglass with mid time deposition (Fg-Mid-dep), fiberglass with long time deposition (Fg-Long-dep), and for comparison the fiberglass without deposition (Fg-no-dep) is also characterized and presented in results section. The produced samples were washed with deionized water and then dried for 1 hour in an oven at 60°C. Figure 1 illustrates the experimental setup.

2.2 - Characterization

The materials were characterized using Transmission Electron Microscopy (TEM) performed in a JEOL JEM-2100 operating at 200 kV, Scanning Electron Microscopy (SEM) with a Jeol JSM-6701F and X-Ray Diffraction (XRD) using a Miniflex II diffractometer, with a Cu kα radiation of 0.15406 Å, set at a 2θ range of 10–90°, with 2° min^{-1} scan speed. The Raman spectra were collected using a MacroRam from Horiba Scientific, with a laser at 785 nm. Atomic Force Microscopy (AFM) was performed in a Multimode 8 from Bruker, under ambient conditions, using Peak Force Tapping mode with ScanAsyst-Air probe - resonant frequency ~ 70 kHz, spring constant ~ 0.4 N/m from Bruker).

3. Results and Discussion

The potential difference established between the electrodes in the evaluated experimental arrangement resulted in the formation of electric arcs between them, as expected. These arcs instantaneously reduced the cyclohexane vapor upon contact. By adjusting the experimental setup (section 2), the reduction process occurred continuously, producing solid reduced material on the surface of the “target substrate”.

The Raman spectroscopy analysis (Fig. 2A) allows us to verify that: (I) due to the increase in deposition time, the Raman signal of the fiberglass structure, which presents a broad peak with a maximum intensity point at 1388 cm^{-1} (red dashed line), was progressively suppressed, and (II) the peaks related to the deposited materials (black dashed line) appeared close to 1328 cm^{-1} and 1585 cm^{-1}, which correspond to graphene D and G bands, respectively [1, 16, 17]. The comparison between Fg-Long-dep (30 min deposition) and Fg-Mid-dep (10 min deposition) allows the verification that the called suppression also occurs at others wavenumber (3253, 2560, 1972, 1765, 1513, 1160, 897, 565 cm^{-1}) of the Raman spectra.

In turn, the 2D band of the deposited materials are located at 2583 cm^{-1}, indicating depositions with few layers [1, 10, 16, 17]. It is interesting to observe that the 2D band appears in Fg-Mid-dep with greater intensity than in Fg-Long-dep, which initially might seem unexpected, since the D and G peaks are more intense in Fg-Long-dep due to the longer deposition time. However, the 2D band is formed due to a resonance event involving photons and is influenced by the structure and stacking of the graphene layers [1]. Thus, it is possible that the characteristics of the deposit obtained, on the curved surface of the fiberglass, have attenuated the resonance as more layers were stacked. This could occur due to a less regular stacking of graphene layers compared to what would happen on flat surfaces and/or due to

structural disorder inducing out-of-phase vibrations, thereby reducing the resonance and consequently the intensity of the 2D peak. This is supported by the defect index (ID/IG) from Raman spectrum. The ID/IG calculated for Fg-Long-dep, which has D and G bands well defined is 1.53, while for Fg-Mid-dep is 1.38 corroborating that the increasing in deposition time could promote increasing in structural disorder. The value of ID/IG obtained for Fg-Short-dep is 1.03; however (although consistent with the others), this measurement may be inaccurate due to the influence of the fiberglass spectral response in this analysis (as stated before). Therefore, since high-quality graphene prepared through the graphite exfoliation method presents ID/IG close to 1.0 [1, 17], and the direct synthesis method used in this study involves the superimposition, reduction, and joining of individual molecules, the obtaining of deposits with some irregularities and defect index until 1.53 can be considered satisfactory.

The infrared analysis (Fig. 2B) shows that the fiberglass exhibits its main spectral response in a peak at 895 cm^{-1} which corresponds to the Si-O-Si bond vibrations. The peak at 695 cm^{-1} concerns to the Si-O bond vibrations. Peaks of low intensity between 1300 and 2400 cm^{-1} correspond to the presence of other oxides, including CO_2 (~ 2350 cm^{-1}) [18] from the analysis room, and a band centered at 3400 cm^{-1} is associated with the Si-OH bond and OH groups [19–21]. Similar to the Raman spectra, the graphene deposits attenuated the response of the fiberglass in the infrared spectra (FTIR), which reduced the intense peaks of the fiberglass below 1200 cm^{-1} and, above this wavenumber, resulted in the obtaining of a noisy baseline.

In graphene synthesized through traditional methods, such as graphite exfoliation, the reactions often introduce oxygenated species into the sheets, resulting in the formation of reduced graphene oxide (RGO). This material can be identified in the infrared (IR) spectrum by characteristic peaks, such as the C–O stretch (1220–1250 cm^{-1}), C = O stretch (1720 cm^{-1}), and O–H stretch (~ 3400 cm^{-1}) [22–24]. Beyond these, a weak peak related to the vibration of C = C sp^2 bonds is typically observed at ~ 1620 cm^{-1} [7, 16, 23–26]. However, in pure graphene, due to the symmetry of its structure, the vibrational modes that appear in the Raman spectrum do not generate a response in the IR spectrum, leading to the absence of well-defined peaks in the IR spectrum [27–29]. Thus, the absence of observable peaks related to oxygenated species and to C-C sp^2 vibration (~ 1620 cm^{-1}) in the infrared spectra (Fig. 2b) suggests that the direct synthesis method, using only cyclohexane and electrons (from the arc) in nitrogen atmosphere, produced graphene without inclusions of oxygenated species.

The X-Ray Diffraction (Fig. 2C) of the fiberglass without any deposition shows an amorphous profile with a broad band of higher intensity around 30° in 2θ. For all fiberglass samples that received graphene deposition, the XRD patterns exhibit a broad band with maximum intensity between 22 and 25° in 2θ, which are attributed to the formation of graphene flakes on these fibers [10, 30]. These broad peaks have low intensities, indicating that the deposits are thin, i.e., correspond to few-layer structures, in agreement with Raman data. Additionally, the increase in deposition time results in a higher intensity of the peak near 22° in 2θ, reflecting an increase in the thickness of the deposited material, which also aligns with Raman observations. Since the X-ray diffraction technique reveals defined peaks only for materials with

regular crystalline structures, the broad and low-intensity pattern observed in Fig. 2c indicates that the deposits made are quite irregular, which also is consistent with Raman data.

In this work, the characteristic random propagation of voltaic arcs (i.e., along the trajectory between two points with lower resistivity [30]), combined with others process variables — such as the concentration and flow of the chemical vapor being reduced at each instant, as well as its mixture with other gases (possibly formed as reaction products in the medium) — results in a point-to-point non-linear increase in material deposition on fiberglass surface over time. Similarly, these features also enable the formation of deposits with various morphologies. Thus, the presentation of micrographs (SEM and AFM) aims to elucidate how the different deposits were obtained.

The micrograph in Fig. 3A shows a fiberglass with little deposits (Fg-short-dep) of graphene (lighter tone structures) in a localized manner. This kind of application is possible because the deposition only occurs when there is the Vapor Precursor of the Deposit (VPD) close to the surface of the target material and this VPD receives the incidence of the voltaic arc. Thus the concentration of the VPD on the 'target surface' and the incidence and intensity of the arc are process variables capable of promote a point-to-point graphene deposition.

By increasing the deposition time, as observed for sample Fg-Mid-dep (Fig. 3B), the deposition becomes more extensive, indicating the stacking of multiple layers of reduced VPD on the 'target surface'. Figure 3C (Fg-long-dep) shows the section (fracture) of a thicker graphene layer, in which can be seen depositions with morphologies varying in roughness and porosity point-to-point. This occurs because, when the voltaic arc remains over the same region of the 'target surface' for several seconds, the gases produced by the reduction of VPD in the presence of N_2 may limit the availability of VPD in that area, and this lack of VPD prevents further deposition. However, when the voltaic arc moves across the surface, the diffusion of VPD inside the electrochemical cell increases its concentration in previously deficient areas, allowing new depositions to occur. Consequently, the movement of the voltaic arc and the structure formed around the last deposition point can make the subsequent deposition occur with a certain 'distance' from the surface of the previous application. Thus, this process results in deposits more or less 'porous' depending on variables such as VPD concentration, N_2 concentration, the products of VPD reduction, and the movement of the voltaic arc.

The images in Fig. 4 demonstrate that, with the appropriate set of variables, graphene deposition can result in a compact structure with strong adhesion. Figure 4A shows several fibers joined by the graphene deposition, and this union was strong enough to prevent their detachment. In fact, these fibers were subjected to mechanical stress aimed at separating them, and the fibers fractured in regions that did not receive any deposition, instead of separating or breaking in areas where the graphene was deposited. This highlights the adhesion strength provided by this graphene deposit. Figures 4B and 4C reveal that the graphene deposition created a three-dimensional structure with several micrometers in length and morphology exhibiting fine and varied details on a fiber. This demonstrates that the process can be refined to achieve deposits with controlled details at smaller scales. It is worth noting that this

structure, despite having small support points relative to its dimensions, remained attached to the fiberglass surface through storage, transportation, and sample preparation for SEM analysis, which is also evidence of the mechanical resistance provided by this compact graphene deposition. The evaluation of mechanical properties, such as adhesion or tension strength, is beyond the scope of this study, but could be addressed with appropriate characterization in future studies.

In order to analyze surface morphology, AFM, a very useful tool for studying topography due to its ability to provide information on the Z scale, was used in Peak Force Tapping mode to obtain data from the samples with and without graphene deposition. The Fb-no-dep sample shows the irregularities of the fiberglass surface, as observed in the height and 3D view images (Figs. 5A and A'). After the deposition process begins, a different structure is formed on the fibers surface, as can be seen in Figs. 5B, C and D. On the left side of Fig. 5B can be seen a structure that is the edge of a graphene deposit. This structural pattern may be attributed to a change in the direction of the voltaic arc during the deposition process along a specific trajectory. By increasing the deposition time and analyzing different regions of the fiber, graphene growth can be observed to occur in an overlapping manner, producing stacked layers. In Fig. 5C, this growth likely occurred when the voltaic arc "oscillated" or "moved" multiple times between two points on the fiber surface, applying layers one by one in each pass along the aforementioned trajectory. Figure 5D shows the intersection between groups of graphene layers formed in two directions, in a "V" shape. This deposition pattern was obtained by the alternated movement of voltaic arc between two trajectories, i.e., after applying graphene layers along one trajectory for some time, the arc changed direction and deposited layers along another trajectory, and so on, resulting in the organized three-dimensional structure. The controlled preparation of this type of graphene structure is particularly promising for electronic devices (e.g., tracks in microprocessors) or biomaterials (e.g., scaffolds for implants).

The white lines in Fig. 5A to 5D represent the trajectory used for the cross-section analysis, with the respective profiles shown in Fig. 5A" to 5D". In the Fb-no-dep sample (Fig. 5A"), which has a curved and irregular surface, these irregularities generally exhibit heights on the order of 10 nm, occasionally reaching values close to 100 nm. As previously mentioned, the formation of graphene structures on the fiberglass surface was achieved through the stacking of several layers. At the edge of the graphene deposits (Fig. 5B"), the heights vary by a few nanometers from point to point and approximately 30 nm between peaks and valleys. Similar structures are observed in the stacked layers shown in Figs. 5C and 5D. In Fig. 5C", the topographic profile reveals graphene layers stacked in a steps-like pattern, with heights ranging from 12 to 56 nm. In turn, the graphene layers alternately stacked in a "V" shape (Fig. 5D") exhibit topographic heights ranging from 24 to 204 nm. These results demonstrate that, under the studied conditions, several layers of graphene were deposited simultaneously. Regarding surface roughness, the root-mean-square (RMS) analyses shows a decrease from 22 nm on the fiberglass surface (dashed square in Fig. 5A) to 1.3 nm on the graphene surface (dashed square in Fig. 5D), an expected result since the graphene surface is smooth.

The results demonstrated that the method was capable of synthesizing graphene directly on the target surface — in this case, the challenging curved, irregular, and hydrophobic surface of fiberglass. Graphene deposits were obtained with diverse thickness, roughness, porosity, and topographic profiles, as well as compact structures with nanometric details. As stated before, the hydrophobic nature of both fiberglass and graphene typically hinders their union to other materials through conventional methods, such as ink formulation and application. However, the method evaluated in this study successfully overcame this obstacle, creating graphene layers strongly bonded to the target surface.

In addition, since voltaic arcs propagate randomly, (along the path between two electrodes with the lowest electrical resistivity), the distance between the electrodes and their shape are variables that could enable greater control over the deposition process. Furthermore, parameters such as the diameter and intensity of the electron beam (generated as a voltaic arc), as well as the flows of VPD and inert gas (N_2), could be optimized to achieve better control over the structure of the deposited material. In this sense, the ability to control gas flows in the voltaic arc trajectory through a specific injection system is an important aspect for future developments. These improvements might enable the synthesis of graphene structures with: (1) selective deposition at specific points on the target surface (creating regions with applied material or empty spaces, as required), and (2) control over the formation and type of pores in the deposited material, both allowing the construction of three-dimensional (3D) structures. This capability of direct graphene synthesis with three-dimensional architecture is promising for applications in electronic devices, bioimplants, and other fields.

As mentioned, during the process, the concentration of VPD can be influenced by gases that could be formed in the medium during VPD reduction, and these gases may limit the continuous supply of VPD to the substrate surface, consequently affecting the characteristics of the deposited material. Thus, the verification of gas formation, their identification and quantification, as well as the assessment of their effects on the characteristics of the deposited material also require further studies. Improvements aimed at eliminating the adverse aspects of these possible gases, as well as developments aimed at controlling their flows or removing them from the medium, may be considered if necessary. The evaluation of these characteristics, as well as the handling and use of this information in controlling deposition and pore formation, should also be addressed in future works.

In parallel with the mentioned efforts to optimize the deposition process, further development focusing on miniaturization could enable this method to fabricate graphene structures with sub-nanometric thicknesses, i.e., dimensions even smaller than those achievable using current lithography with gold or other materials [31].

In both cases, the establishment of a finely controlled material deposition method based on voltaic arcs would offer advantages over Physical Vapor Deposition (PVD) and Chemical Vapor Deposition (CVD), because such a method enables the creation of structures with morphological characteristics controlled point by point. A technique with these features could open new possibilities for the development of devices and applications of graphene with customized properties for diverse technology fields.

4. Conclusion

The conducted study demonstrated that, despite being subject to optimization, the method is capable of producing pure graphene structures with diverse morphologies and topographic profiles even on challenging surfaces, such as the glass fiber cloth used as the target substrate. The various characteristics observed under the different deposition conditions could be clearly correlated with the process parameters. Through developments, this technique could give rise to systems for localized application of graphene (or other 2D materials) on other surfaces, with shapes and morphology controlled “point by point”, which is of broad interest to various industry sectors, especially for applications in microelectronics and biomaterials.

Declarations

Author Contribution

All authors contributed to the experimental work and/or manuscript preparation. All authors approve the manuscript and agree with its submission for publication.

Acknowledgment

We are grateful to CAPES, CNPq [350514/2023-2, 302709/2020-7], COPDE/IPEN [2020.06.IPEN.05.PD, 2020.06.IPEN.22.PD] for financial support.

Conflicts of Interest: There is no conflict of interest.

Data Availability

Additional data can be obtained upon reasonable request to the authors.

References

1. Xie, X., Zhou, Y., Huang, K. (2019) Advances in microwave-assisted production of reduced graphene oxide. Front. Chem. 355 (2019), 7. https://doi.org/10.3389/fchem.2019.00355.
2. Yingpeng Wu, Bin Wang, Yanfeng Ma, Yi Huang, Na Li, Fan Zhang, Yongsheng Chen. Efficient and Large-Scale Synthesis of Few-Layered Graphene Using an Arc-Discharge Method and Conductivity Studies of the Resulting Films. Nano Res. 2010, 3(9): 661–669. https://doi.org/10.1007/s12274-010-0027-3.
3. Zhongshan Lu, Cheng Wang, Xianhui Chen, Ming Song, Weidong Xia. Effects of buffer gas on N-doped graphene in a non-thermal plasma process. Diamond & Related Materials 118 (2021) 108548. https://doi.org/10.1016/j.diamond.2021.108548.

4. Cheng Wang, ZhongShan Lu, Jing Ma, Xianhui Chen, Chengpeng Yang, Weidong Xia. Pressure-dependent synthesis of graphene nanoflakes using Ar/H2/CH4 non-thermal plasma based on rotating arc discharge. Diamond & Related Materials 111 (2021) 108176. https://doi.org/10.1016/j.diamond.2020.108176.
5. Baoshou Shen, JijunDing, XingbinYan, WangjunFeng, Jun Li, Qunji Xue. Influence of different buffer gases on synthesis of few-layered graphene by arc discharge method. Applied Surface Science 258 (2012) 4523–4531. https://doi.org/10.1016/j.apsusc.2012.01.019.
6. Gokçe Borand, Nazlı Akçamlı, Deniz Uzunsoy. Structural characterization of graphene nanostructures produced via arc discharge method. Ceramics International 47 (2021) 8044–8052. https://doi.org/10.1016/j.ceramint.2020.11.158.
7. Nan Li, Zhiyong Wang, Keke Zhao, Zujin Shi, Zhennan Gu, Shukun Xu. Large scale synthesis of N-doped multi-layered graphene sheets by simple arc-discharge method. Carbon 48 (2010) 255–259. https://doi.org/10.1016/j.carbon.2009.09.013.
8. K. S. Subrahmanyam, L. S. Panchakarla, A. Govindaraj, C. N. R. Rao. Simple Method of Preparing Graphene Flakes by an Arc-Discharge Method. The Journal of Physical Chemistry C 2009 113 (11), 4257–4259. https://pubs.acs.org/doi/10.1021/jp900791y.
9. Yani Chen, Hongbin Zhao, Leimei Sheng, Liming Yu, Kang An, Jiaqiang Xu, Yoshinori Ando, Xinluo Zhao. Mass-production of highly-crystalline few-layer graphene sheets by arc discharge in various H2–inert gas mixtures. Chemical Physics Letters 538 (2012) 72–76. http://dx.doi.org/10.1016/j.cplett.2012.04.020.
10. Gomes, P.V.R., Bonifacio, R.N., Silva, B.P.G., Ferreira, J.C., de Souza, R.F.B., Otubo, L., Lazar, D.R.R., Neto, A.O. (2023) Graphene Deposited on Glass Fiber Using a Non-Thermal Plasma System. Eng. 4, 2100–2109, https://doi.org/10.3390/eng4030119
11. Stickel, J. M., Nagarajan, M. (2012) Glass Fiber-Reinforced Composites: From Formulation to Application. Int. J. of Appl. Glass Sci. 3, 122–136. https://doi.org/10.1111/j.2041-1294.2012.00090.x
12. Khazanov, V.E., Kolesov, Y.I., Trofimov, N.N. (1995) Glass fibres. In: Kostikov, V.I. (ed.) Fibre Science and Technology. vol 5, 15–230, Springer, Dordrecht. https://doi.org/10.1007/978-94-011-0565-1_2
13. Wazeer, A., Das, A., Abeykoon, C., Sinha, A., Karmakar, A. (2023) Composites for electric vehicles and automotive sector: A review. Green Energy and Intelligent Transportation, 2 (1) 100043. https://doi.org/10.1016/j.geits.2022.100043
14. Mohammadi, H., Ahmad, A., Mazlan, S.A., Johari, M.A.F., Siebert, G., Petrů, M., Koloor, S.S.R. (2023) Lightweight Glass Fiber-Reinforced Polymer Composite for Automotive Bumper Applications: A Review. Polymers, 15, 193. https://doi.org/10.3390/polym15010193
15. Sreejith, M., Rajeev, R.S. (2021) “25 - Fiber reinforced composites for aerospace and sports applications. ” In: K. Joseph, K. Oksman, G. George, R. Wilson, S. Appukuttan (eds) Fiber Reinforced Composites. Constituents, Compatibility, Perspectives, and Applications, pp. 821–859, Woodhead

Publishing Series in Composites Science and Engineering. https://doi.org/10.1016/B978-0-12-821090-1.00023-5

16. Wu, W., Liu, M., Gu, Y., Guo, B., Ma, H., Wang, P., Wang, X., Zhang, R. (2020) Fast chemical exfoliation of graphite to few-layer graphene with high quality and large size via a two-step microwave-assisted process. Chemical Engineering Journal, 381, 122592. https://doi.org/10.1016/j.cej.2019.122592
17. Ranjan, P., Agrawal, S., Sinha, A., Rao, T.R., Balakrishnan, J., Thakur, A.D. (2018) A Low-Cost Non-explosive Synthesis of Graphene Oxide for Scalable Applications. Sci. Rep. 8, 12007. https://doi.org/10.1038/s41598-018-30613-4
18. Ngohang, F.E., Fontaine, G., Gay, L., Bourbigot, S. (2014) Revisited investigation of fire behavior of ethylene vinyl acetate/aluminum trihydroxide using a combination of mass loss cone, Fourier transform infrared spectroscopy and electrical low pressure impacto. Polymer Degradation and Stability, 106, 26–35. https://doi.org/10.1016/j.polymdegradstab.2014.01.019
19. Xu, B., Long, J., Xu, G., Yang, J., Liang, Y., Hu, J. (2019) Facile fabrication of superhydrophobic and superoleophilic glass-fiber fabric for water-in-oil emulsion separation. Textile Research Journal, 89, 2674–2681. https://doi.org/10.1177/0040517518801189
20. Mhatre, A.M., Chappa, S., Ojha, S., Pandey, A.K. (2019) Functionalized glass fiber membrane for extraction of iodine species. Separation Science and Technology, 54, 1469–1477. doi: 10.1080/01496395.2018.1520729
21. Bonon, A.J., Weck, M., Bonfante, E.A., Coelho, P.G. (2016) Physicochemical characterization of three fiber-reinforced epoxide-based composites for dental applications. Materials Science and Engineering C, 69, 905–913. https://doi.org/10.1016/j.msec.2016.07.002.
22. Daniela C. Marcano, Dmitry V. Kosynkin, Jacob M. Berlin, Alexander Sinitskii, Zhengzong Sun, Alexander Slesarev, Lawrence B. Alemany, Wei Lu, James M. Tour. Improved Synthesis of Graphene Oxide. Acs nano vol. 4. 8. (2010) 4806–4814. https://doi.org/10.1021/nn1006368.
23. Iskandar, F., Hikmah, U., Stavila, E., Aimon, A.H. (2017) Microwave-assisted reduction method under nitrogen atmosphere for synthesis and electrical conductivity improvement of reduced graphene oxide (rGO). RSC Adv., 7, 52391–52397. https://doi.org/10.1039/C7RA10013B.
24. Fernández-Merino, M.J., Guardia, L., Paredes, J.I., Villar-Rodil, S., Solís-Fernández, P., Martínez-Alonso, A., Tascón, J.M.D. (2010). Vitamin C Is an Ideal Substitute for Hydrazine in the Reduction of Graphene Oxide Suspensions. J. Phys. Chem. C. 114, 6426–6432. https://doi.org/10.1021/jp100603h.
25. Shi, Y., Li, C., Shen, L., Bao, N. (2021) Structure-dependent re-dispersibility of graphene oxide powders prepared by fast spray drying. Chinese Journal of Chemical Engineering, 32, 485–492. https://doi.org/10.1016/j.cjche.2020.08.023.
26. Hayyan, M., Abo-Hamad, A., AlSaadi, M.A. et al. Functionalization of graphene using deep eutectic solvents. Nanoscale Res. Lett. 10, 324 (2015). https://doi.org/10.1186/s11671-015-1004-2.
27. Roland Gillen, Marcel Mohr, and Janina Maultzsch. Symmetry properties of vibrational modes in graphene nanoribbons. Physical Review B81 (2010) 205426.

https://doi.org/10.1103/PhysRevB.81.205426.

28. D. N. Basov and M. M. Fogler. Colloquium: Graphene spectroscopy. Reviews of modern physics, volume 86, 2014. https://doi.org/10.1103/RevModPhys.86.959.
29. Yonghao Liu; Arvinder Chadha; Deyin Zhao; Jessica R. Piper; Yichen Jia; Yichen Shuai; Laxmy Menon; Hongjun Yang; Zhenqiang Ma; Shanhui Fan; Fengnian Xia; Weidong Zhou. Approaching total absorption at near infrared in a large area monolayer graphene by critical coupling. Appl. Phys. Lett. 105, (2014)181105. https://doi.org/10.1063/1.4901181.
30. Sieradzka, M., Slusarczyk, C., Fryczkowski, R., Janicki, J. (2020) Insight into the effect of graphite grain sizes on the morphology, structure and electrical properties of reduced graphene oxide. j. mater. res. technol., 9, 7059–7067. https://doi.org/10.1016/j.jmrt.2020.05.026.
31. Iason Giannopoulos, Iacopo Mochi, Michaela Vockenhuber, Yasin Ekinci, Dimitrios Kazazis. Extreme ultraviolet lithography reaches 5 nm Resolution. Nanoscale, 16 (2024) 15533. https://doi.org/10.1039/D4NR01332H.

Figures

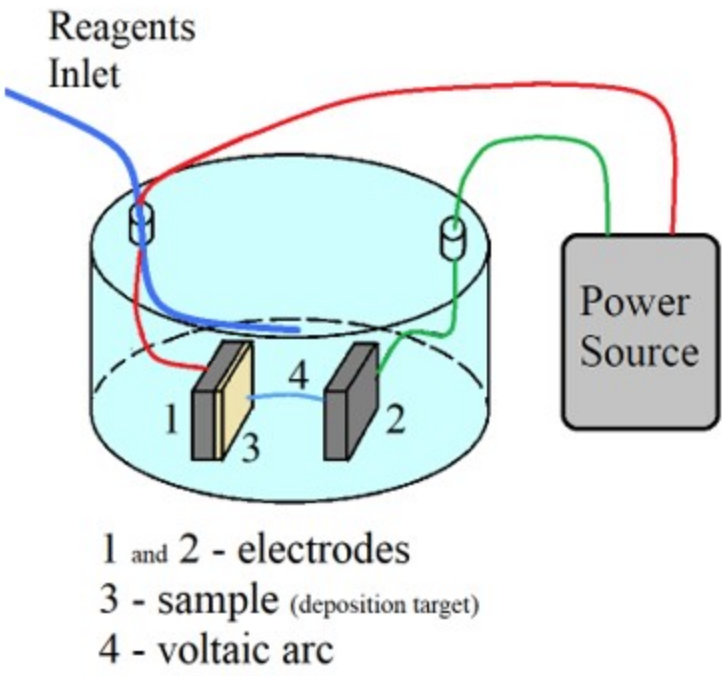

Figure 1

Illustration of the experimental setup for graphene direct synthesis.

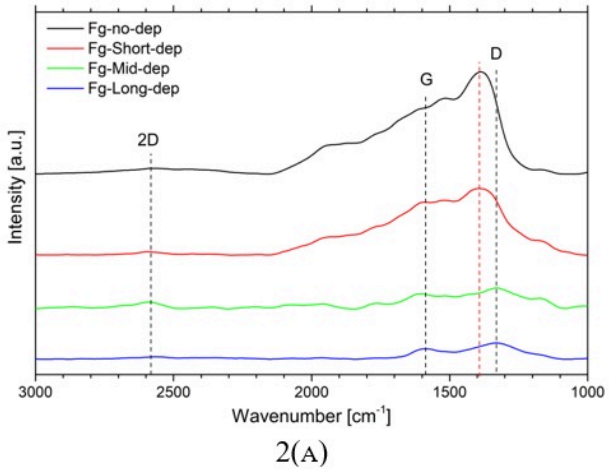

2(A)

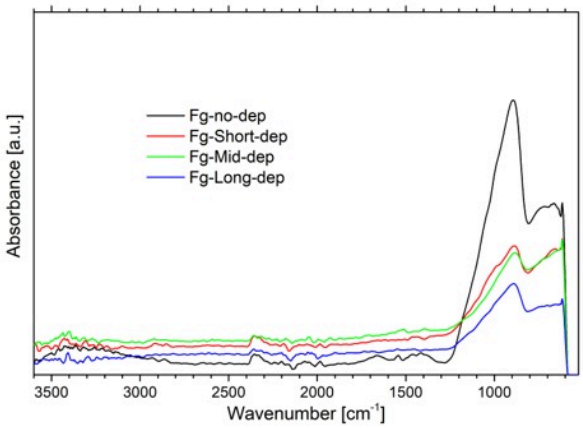

2(B)

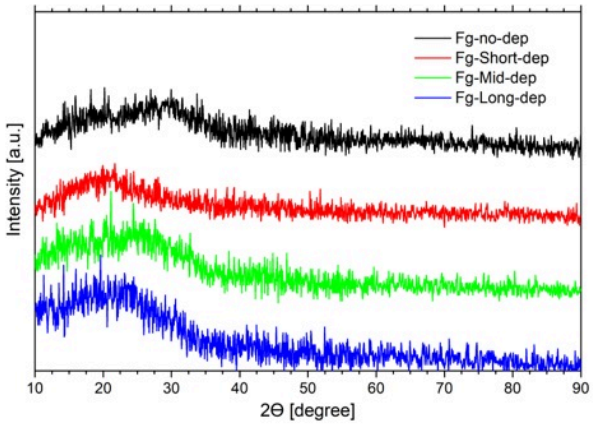

2(C)

Figure 2

Analysis of fiberglass with and without graphene depositions: (A) Raman spectroscopy, (B) Infrared spectroscopy, and (C) X-ray diffraction.

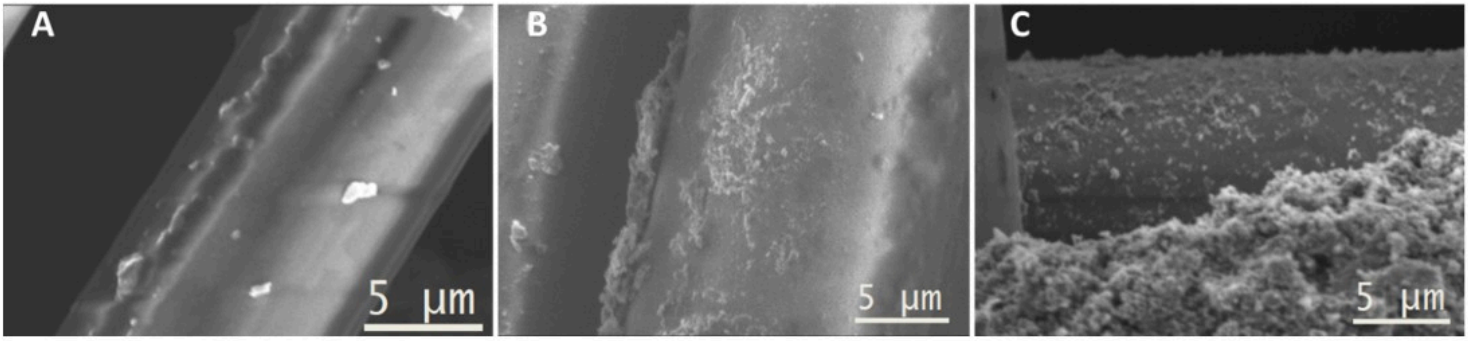

Figure 3

SEM images of (A) Fg-short-dep; (B) Fg-Mid-dep; (C) Fg-Long-dep.

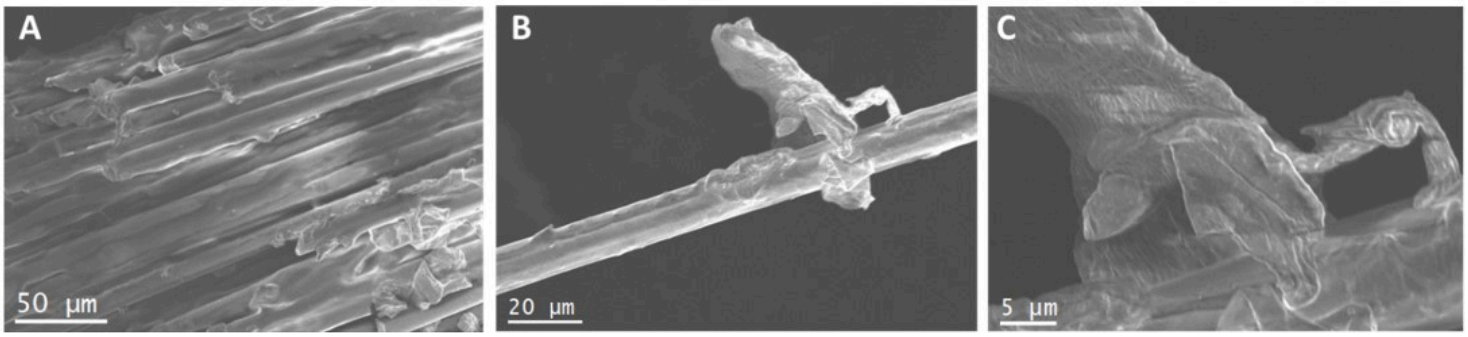

Figure 4

SEM images of Fg-Long-dep.

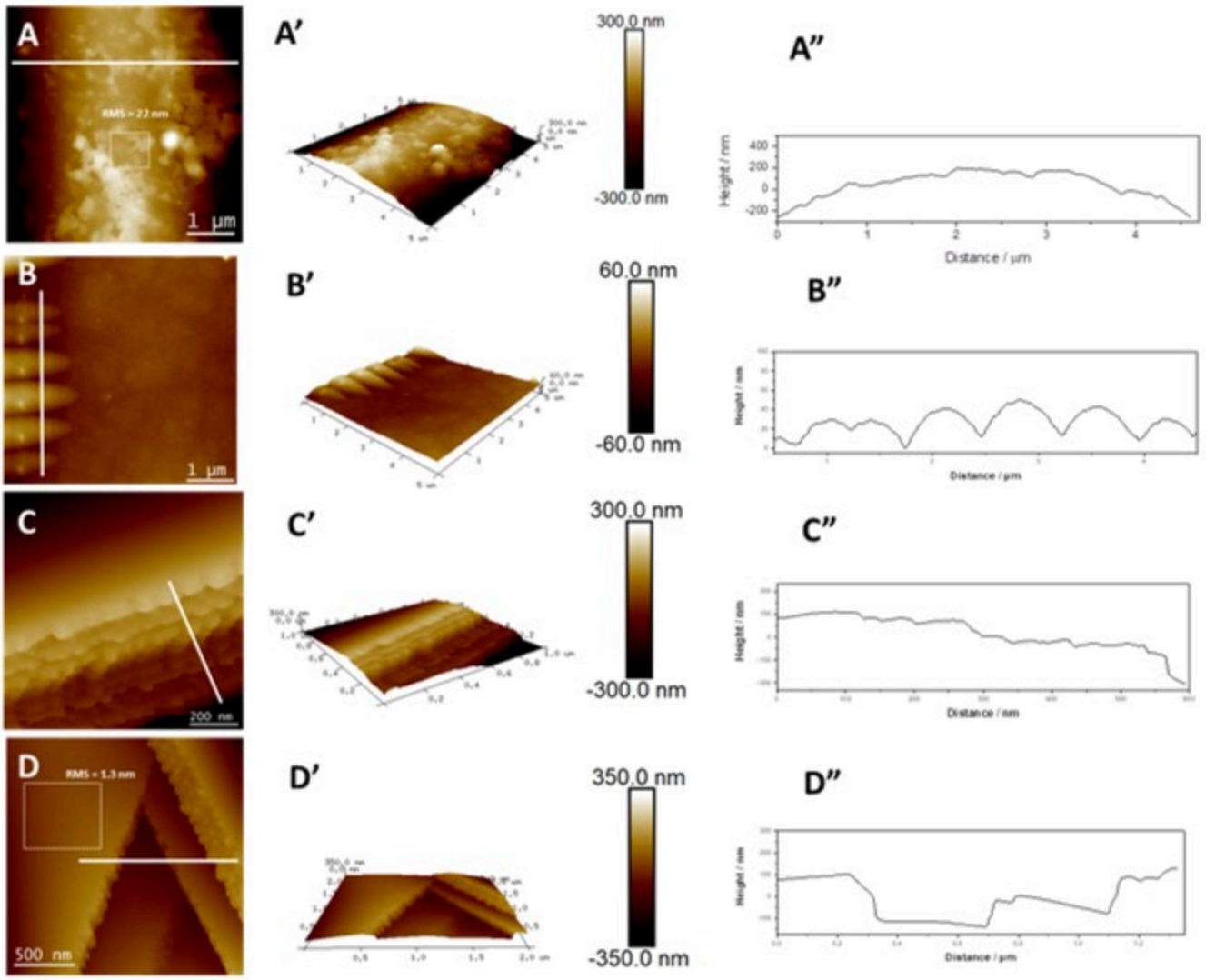

Figure 5

AFM images obtained in Peak Force Tapping mode for Fb-no-dep (A to A”), fiberglass with graphene deposit edges (B to B”), fiberglass with graphene deposited in multiple layers (C to C”), and fiberglass with groups of graphene layers alternately stacked in two directions (D to D”). The images are presented as Height maps (A to D), 3D views (A’ to D’), and cross-section profiles along the indicated lines in the respective images (A” to D”).